Journal of
Water & Climate Change

IWA PUBLISHING

Journal of Water and Climate Change Vol 12 No 8, 3734 doi: 10.2166/wcc.2021.187

Spreading of the semi-arid climate across South Africa

Mark R. Jury [a,b]

[a] University of Zululand, KwaDlangezwa, South Africa
[b] University of Puerto Rico, Mayagüez, USA
E-mail: mark.jury@upr.edu

MRJ, 0000-0002-6871-403X

ABSTRACT

The eastward shift of semi-arid climate across South Africa is studied using satellite assimilated cloud cover, vegetation temperature and potential evaporation 1981–2019, and 21st century coupled model projections. Semi-arid thresholds over the plateau have shifted hundreds of kilometers eastward in the Vaal River catchment for potential evaporation, cloud fraction, and vegetation temperature. Coastal cloudiness has also changed due to sea breezes modified by shelf zone sea temperatures. Processes underlying the spread of semi-arid conditions across South Africa are quantified. Desiccation is related to greater westerly airflow, as the atmospheric boundary layer over the Kalahari preferentially links with the upper-level circulation. Warm dry spells and climate change enhance the meridional temperature gradient and accelerate the sub-tropical jet at both short- and long timescales. According to observations and reanalysis, dry westerlies prevail during the afternoon and induce +0.2 °C/year trends in vegetation temperature over the Highveld during the study period. Coupled model projections show that semi-arid conditions expand eastward from Bloemhof (25.5°E) by 50,000 km^2, altering future adaptation strategies.

Key words: coupled model projections, eastward drying trend, satellite measurements, South Africa

HIGHLIGHTS

- The semi-arid climate of South Africa is studied using high-resolution satellite datasets 1981–2019 and 21st century coupled model projections.
- Semi-arid thresholds over the plateau have shifted hundreds of kilometers southeastward.
- A westerly airflow over the Kalahari joins with the sub-tropical jet to export warm dry air to the escarpment, particularly in the afternoon.

1. INTRODUCTION

The semi-arid climate of South Africa can be traced to high elevation, a sub-tropical latitude, and the inflow of dry air from the South Atlantic (Vigaud *et al.* 2009) which is prominent during winter and in the Pacific El Niño phase. Moisture is locally dissipated via evaporative fluxes compounded by anthropogenic stress (Chikoore & Jury 2010).

Understanding shifts in climate can forewarn of socio-economic consequences that could be mitigated by adaptive resource management (Tyson & Crimp 1998; Scholes *et al.* 2002; Ringrose *et al.* 2003). Past research has found trends of ~0.02 °C/year in air temperatures (Jury 2018) consistent with global averages, but regional studies on evaporative stress under climate change are limited. It is conjectured that the Kalahari Desert is spreading eastward into agriculturally productive lands, threatening livelihoods and resources in southern Africa (Tyson & Crimp 1998), presenting a motivation for this research. Scientific advances via satellite data assimilation offer insights on feedback between vegetation, clouds, moisture budget, and the radiative balance (Bounoua *et al.* 2000) and provide ways to link historical trends to underlying processes. Coupled model intercomparison project (CMIP) resources (Taylor *et al.* 2011) enable long-range projections of climatic shifts as a basis for informed decisions on mitigating actions.

Although some coupled models under-represent the mean state and annual cycle (Munday & Washington 2018), bias-adjusted comparisons with observed trends offer guidance on climate change that exceeds multi-decadal oscillations (Mann *et al.* 2020). Engelbrecht & Engelbrecht (2016) analyzed shifts in Koppen classification zones over southern Africa using downscaled CMIP3 model projections. Under 3 °C global temperature increase from baseline, a southeastward

expansion of warm dry 'B' semi-arid Koppen climate zones from 72 to 90% of land cover was found. The temperate 'C' sub-humid seasonal Koppen climate zones of South Africa contracted commensurately.

The main objective of this research is to determine the pattern and causes of an eastward shift of semi-arid climate across South Africa since 1981 and to analyze whether that trend may continue into the future. Section 2 outlines the data and methods utilized. In Section 3, the results cover shifts in semi-arid thresholds across South Africa: 36–23°S, 16–34°E, underlying processes, observed trends, and hydrology projections. Section 4 closes with a summarizing discussion. This work is novel, in that it employs satellite measurements of vegetation temperature and cloud cover, and surface moisture balance via reanalysis and coupled models to provide a coherent view of gradual changes in climate.

2. DATA AND METHODS

South Africa and its shelf zone are well observed by weather stations and shipping lanes. Satellites provide global coverage at 5 km resolution and modern assimilation systems calibrate and blend these measurements with *in situ* data to provide a 40-year history of climate for the evaluation of shifts and trends that may be natural or anthropogenic. A flow chart (Figure 1) outlines the sequence of methods; all dataset acronyms are defined in Table 1.

2.1. Data and sources

The interpolated satellite products include Eumetsat net solar radiation and cloud fraction (Eumetsat 2021a, 2021b) and NOAA vegetation temperature (NESDIS 2021) and sea surface temperature (SST). The 5 km resolution Eumetsat net solar radiation depends on calculated sun angle, surface and cloud 0.5–1.1 μm emissivity from geostationary satellite, and vertically integrated water vapor, ozone, and aerosols for transmissivity. The 25 km resolution Eumetsat cloud fraction uses

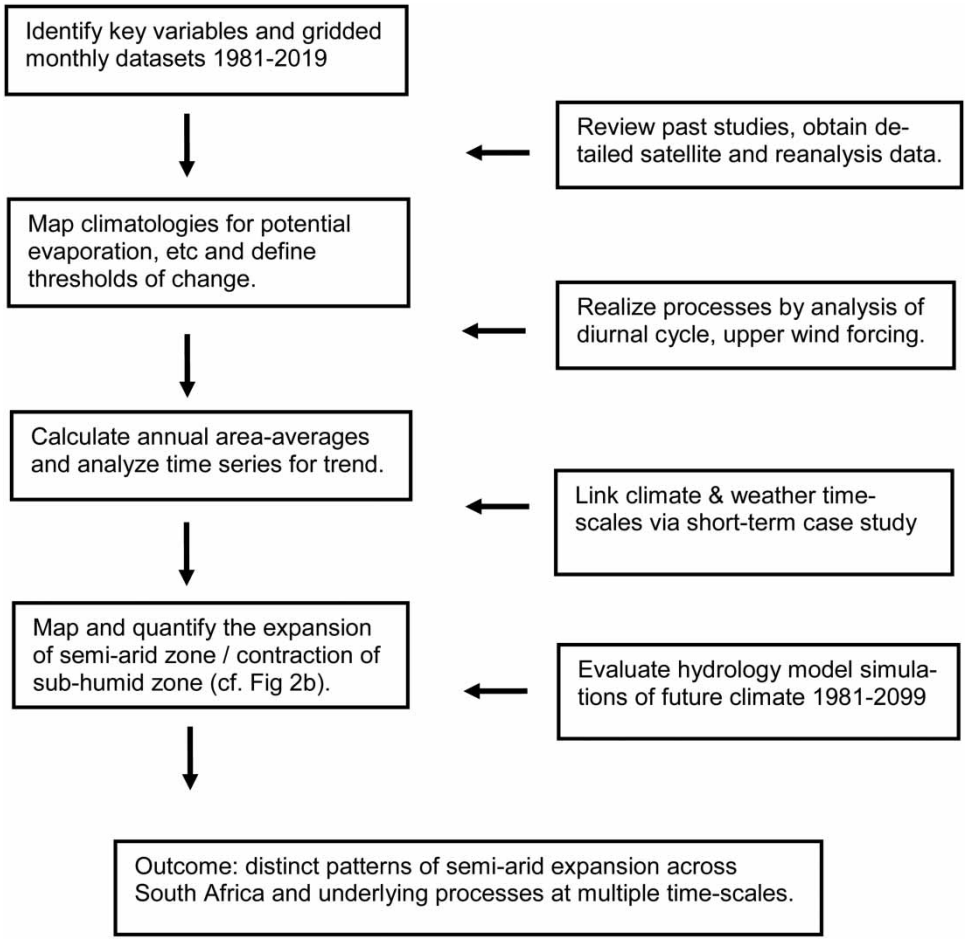

Figure 1 | Flow chart of methods.

Table 1 | Datasets used in the analysis

Acronym	Name	Resolution
CFS2	Coupled Forecast System Reanalysis v2, winds	25 km
Dept Water Affairs	South Africa hydrology service, station S-pan observations	Bloemhof
ERA5	European Centre Reanalysis v5 hourly weather parameters	25 km
Eumetsat	European meteorology satellite center, solar radiation and cloud fraction	5–25 km
GLOFAS	River discharge reanalysis from European Centre	10 km
HADgem2-ISIMIP	Hadley Centre simulation for the Inter-Sectoral Impact Model Intercomparision Project v2	50 km
H08, LPjml, Watergap	Hydrology submodels associated with the HADgem2-ISIMIP simulation	50 km
MERRA2	Modern Era Reanalysis for Research and Applications v2 (NASA)	50 km
NOAA-NESDIS	National Oceanic & Atmospheric Administration – environmental satellite data information service SST and veg.temp.	1–16 km
SAWS	South Africa Weather Service station profile/wind observations	Bloemfontein DeAar

References are listed in the text, web sources are given in the acknowledgement.

multiple polar-orbiting satellite 11 μm radiance data to distinguish cloudy pixels from background and sum the binary frequency over time. The 16 km resolution NOAA-NESDIS vegetation temperature and SST uses de-clouded 11 μm emissivity from multiple polar-orbiting satellites averaged to monthly value. All datasets are listed in Table 1.

CFS2, ERA5, and MERRA2 coupled reanalyses (Saha *et al.* 2010; Rienecker *et al.* 2011; Saha *et al.* 2014; Molod *et al.* 2015; Hersbach *et al.* 2020, respectively) are used to describe the wind, air and dewpoint temperature, specific humidity, sensible and latent heat flux, boundary layer height, and soil moisture at 25–50 km resolution. Potential evaporation is a critical variable that describes moisture dissipation via sensible heat flux and compares favorably with S-pan measurements (Jury 2016). Rainfall is of less value here, as it cannot describe moisture losses and desertification. Similarly, evapotranspiration or latent heat flux that describes moisture recycling is of limited value. Table 1 defines the data resolution, in-text references cover validations, and acknowledgements list the internet sources.

2.2. Methods and models

Annual averages are used in most analyses, given how moisture deficits accumulate over the dry season and affect the lower atmosphere (Keys *et al.* 2016). Climatology and linear regression trends are mapped across South Africa (36–23°S, 16–34°E) during the satellite era 1981–2019. A threshold analysis is conducted to identify the eastward expansion of the semi-arid climate regime, using January 2001 as the break-point separating the first and second half of record, each having a similar number of wet and dry years. The thresholds used to describe regime shifts are 4.3–4.7 mm/day for potential evaporation, 39–42% for cloud fraction, and 25–28 °C for vegetation temperature. These were subjectively assigned based on proximity to key geographic features in the Vaal River catchment.

Temporal analyses were extracted for the Bloemhof Reservoir on the Vaal River (27.7°S, 25.7°E) and include GLOFAS naturalized discharge (Harrigan *et al.* 2020), reanalysis variables, and 1 km resolution satellite measurements of land surface and water temperatures. South African Department of Water Affairs S-pan observations and maximum temperatures were obtained near Bloemhof. Projections of potential evaporation are provided by the 50 km resolution HADgem2-ISIMIP model (Frieler *et al.* 2018) with RCP6 scenario (moderate emission pathway to doubling of CO_2). This coupled model was employed because of its ability to simulate the distribution, annual cycle, and trends of African climate (Engelbrecht & Engelbrecht 2016; Munday & Washington 2018; Thomas & Nigam 2018). Coupled model projections from HADgem2 along the 25.5°E section were analyzed for surface air temperature (reduced to sea level, e.g. potential) and zonal winds. Changes in potential evaporation at Bloemhof were evaluated for three hydrology submodels: H08, LPjml, and Watergap (Hanasaki *et al.* 2008; Müller *et al.* 2014; Jagermeyr *et al.* 2015, respectively) in the period 1981–2099; the linear trend slope and r^2 fit were determined. Field significance above 98% confidence governs interpretations.

2.3. Understanding causes and quantifying changes

Having determined impacts, exploratory analyses on causal mechanisms found that low-level westerly winds tend to accelerate over the southern plateau during warm dry spells, particularly in the afternoon. Weather station wind roses at DeAar (30.7°S, 24.0°E) were calculated in the period 2001–2019 for all hours and for 14:00–20:00 h (N = 46,000 and 12,000). Diurnal 'residual' departures from all-hour means were calculated for MERRA2 near-surface hourly zonal winds in the period January 2014–December 2019 (N = 1,825 per hour) and plotted as a mean diurnal cycle Hovmöller on a north-south slice. Similarly, diurnal residual height sections on 25.5°E of 14:00–20:00 h were analyzed for MERRA2 zonal wind and air temperature in the layer up to 700 hPa. Hourly reanalysis data at Bloemhof from CFS2, ERA5, and MERRA2 were analyzed to identify the thermally driven wind response during the summer of December–February 2016 (N = 91 per hour). The warm dry case of 6 January 2016 was studied for its extreme wind and temperature patterns, accompanied by the radiosonde profile at Bloemfontein 29.1°S and 26.3°E.

Semi-arid thresholds were mapped for the first and last 20 years, and comparative statistics were gathered. To quantify the shift in climate, the number of 0.5° squares exceeding the designated thresholds for potential evaporation, cloud fraction, and vegetation temperature was counted. This was done for reanalysis and projected fields in three periods: 1981–2000, 2001–2019, and 2080–2099. Statistics were gathered using the grid illustrated in Figure 3(b): expansion of the dry edge from 25.5°E longitude, and contraction of the wet edge from the southeast coast. Similar methods were employed by Engelbrecht & Engelbrecht (2016) to describe model-projected changes in Koppen climate regimes over South Africa.

3. RESULTS AND DISCUSSION

The results progress from climatology and trend maps to shifts in semi-arid thresholds across South Africa, then to the underlying processes involving diurnal advection and observed trends, and finally to hydrology projections and inter-comparisons.

3.1. Climatology, trend, and threshold maps

The 1981–2019 climatology of satellite vegetation temperature (Tveg) and net solar radiation (Qs) and their respective linear trend maps are presented in Figure 2(a)–2(d). The expected east-cool-cloudy/west-warm-sunny pattern is evident in the climatology maps, largely controlled by the regional SST pattern. Qs trends are upward +0.2 W m^{-2}/year except for the eastern coastal plains. The Tveg trends are upward +0.2 °C/year along the southern edge of the plateau, aligned with gradients of mean air temperature. Over the Orange River Valley and Eastern Cape coast, Tveg trends are weak. A close-up of Qs trends for Cape Town and Durban areas (Figure 2(e) and 2(f)) suggests that sea breezes modified by shelf zone SST trends (Figure 2(g)) lead to a sun-belt in the west and a cloud-belt in the east. Benguela coastal upwelling in the southwest enhances subsidence, whereas warming of the Agulhas Current enhances rising motion. Further inland, the 850–700 hPa winds have become more westerly over the period 1981–2019.

Figure 3(a)–3(c) illustrates before and after maps using 2001 as the break-point. Although a variety of fields are analyzed for semi-arid threshold, they reflect a similar eastward expansion of sunny, dry, and warm conditions from before to after (1981–2000/2001–2019). There are southward expansion of semi-arid thresholds in Western Cape longitudes of 18–24°E from 33 to 33.5°S, and eastward expansion in Free State latitudes of 24–31°S from 26 to 27°E. In some maps, the semi-arid range broadens, most prominently for Tveg in Limpopo, Lubombo, and Tugela Valleys. The lower Vaal catchment (Bloemhof) provides a geographic reference for the eastward shift.

3.2. Diurnal processes

Potential evaporation depends on turbulence generated by high temperatures and winds, compelling an analysis of the mean diurnal cycle. The Hovmöller plot of zonal wind on 25.5°E (Figure 4(a)) shows residual easterlies over the plateau at night. A few hours after sunrise westerlies accelerate over the escarpment and spread inland. During peak heating at 13:00 h, the residual westerlies reach 3 m/s. Around sunset, easterlies resume over the escarpment.

Afternoon height sections on 25.5°E of residual air temperature and zonal wind (Figure 4(b) and 4(c)) show a tilted warm layer of +2 °C inducing +2 m/s westerlies that are strongest from 26 to 28°S above 800 hPa. The afternoon residual low-level specific humidity and wind map (Figure 4(d)) reveals a broad arc of westerlies sweeping Kalahari air toward the escarpment, creating a pattern similar to the trend of Tveg (cf. Figure 2(b)). Afternoon sea breezes contain the drying trend to the escarpment.

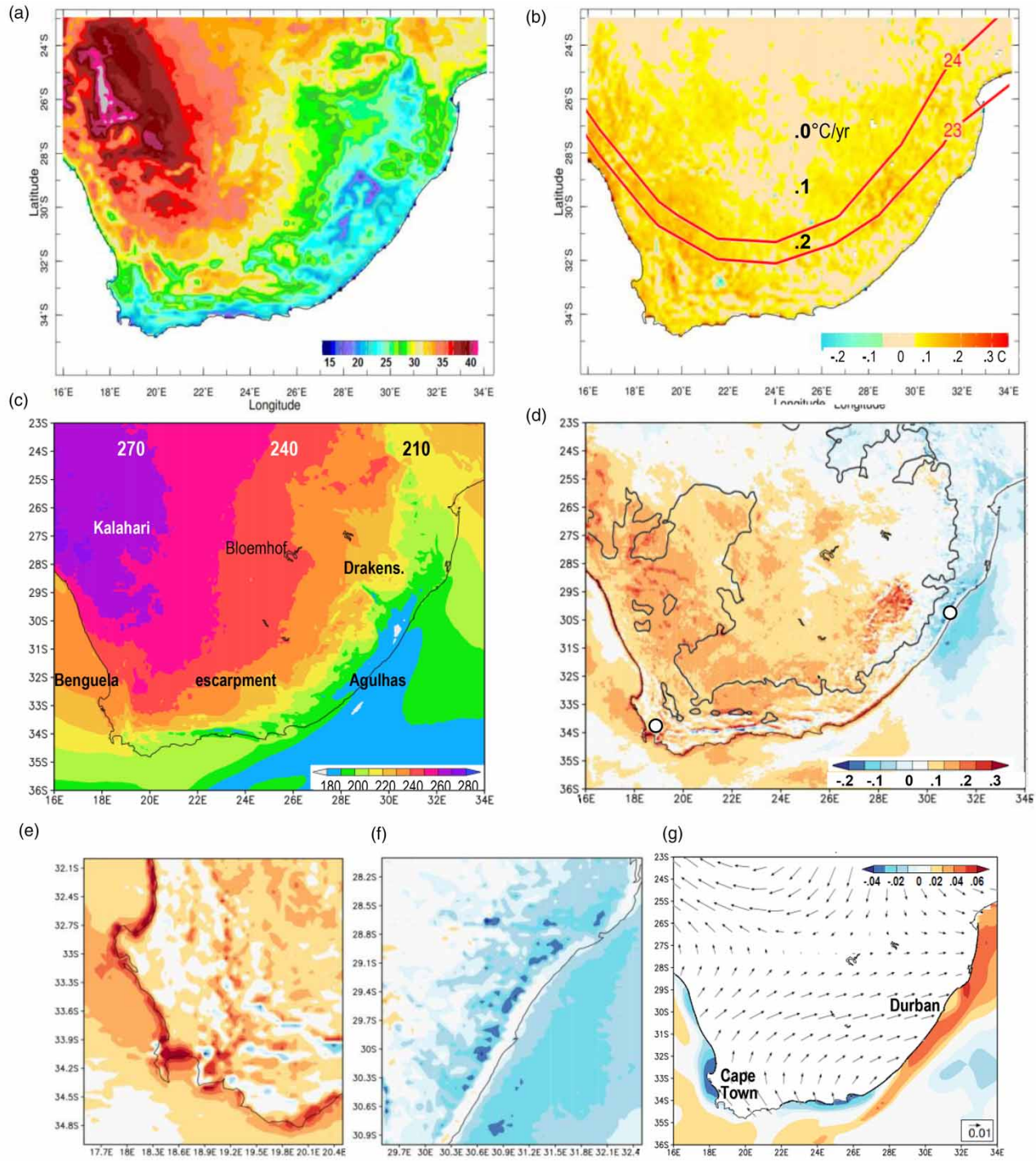

Figure 2 | (a) 1981–2019 climatology of vegetation temperature and (b) its linear trend (°C/year) with mean 925 hPa isotherms. (c) Climatology of net solar radiation with geographic labels and (d) its linear trend (W m^{-2}/year) with 1,000 m elevation contour. Close-up of same linear trend for (e) Cape Town and (f) Durban coastal areas. (g) SST trend for shelf zone (°C/year) and 850–700 hPa wind trends over land (m s^{-1}/year).

The diurnal export of warm dry air across the plateau underpins an eastward shift of semi-arid conditions. DeAar weather station wind roses 2001–2019 stratified for all hours and afternoon only (Figure 5(a), Table 2) show that westerlies occur more than half the time from 14:00 to 20:00 h. Southeasterlies prevail at night and early morning; overall mean wind speeds of 4.4 m/s increase to 5.8 m/s in the afternoon.

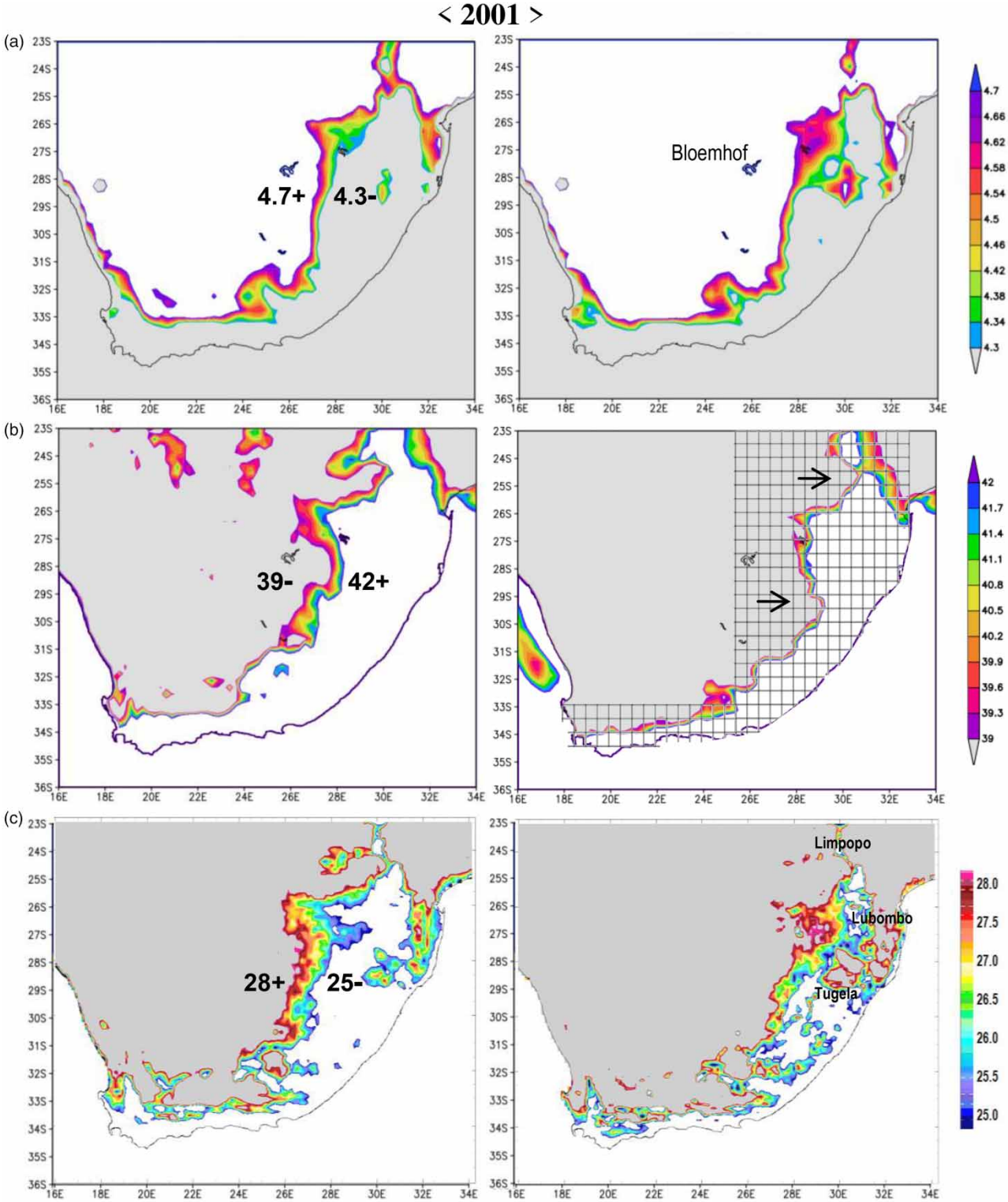

Figure 3 | Before 2001 (left) and after (right) patterns for semi-arid thresholds: (a) potential evaporation (mm/day), (b) cloud fraction (%), and (c) vegetation temperature (°C) (with eastern valleys labeled). Shading refers to blue = cool moist and red = warm dry. The Bloemhof reservoir is labeled in (a) right, arrows highlight eastward shift in (b) right, which includes the 0.5° matrix to quantify semi-arid expansion and sub-humid contraction. Please refer to the online version of this paper to see this figure in color: http://dx.doi.org/10.2166/wcc.2021.187.

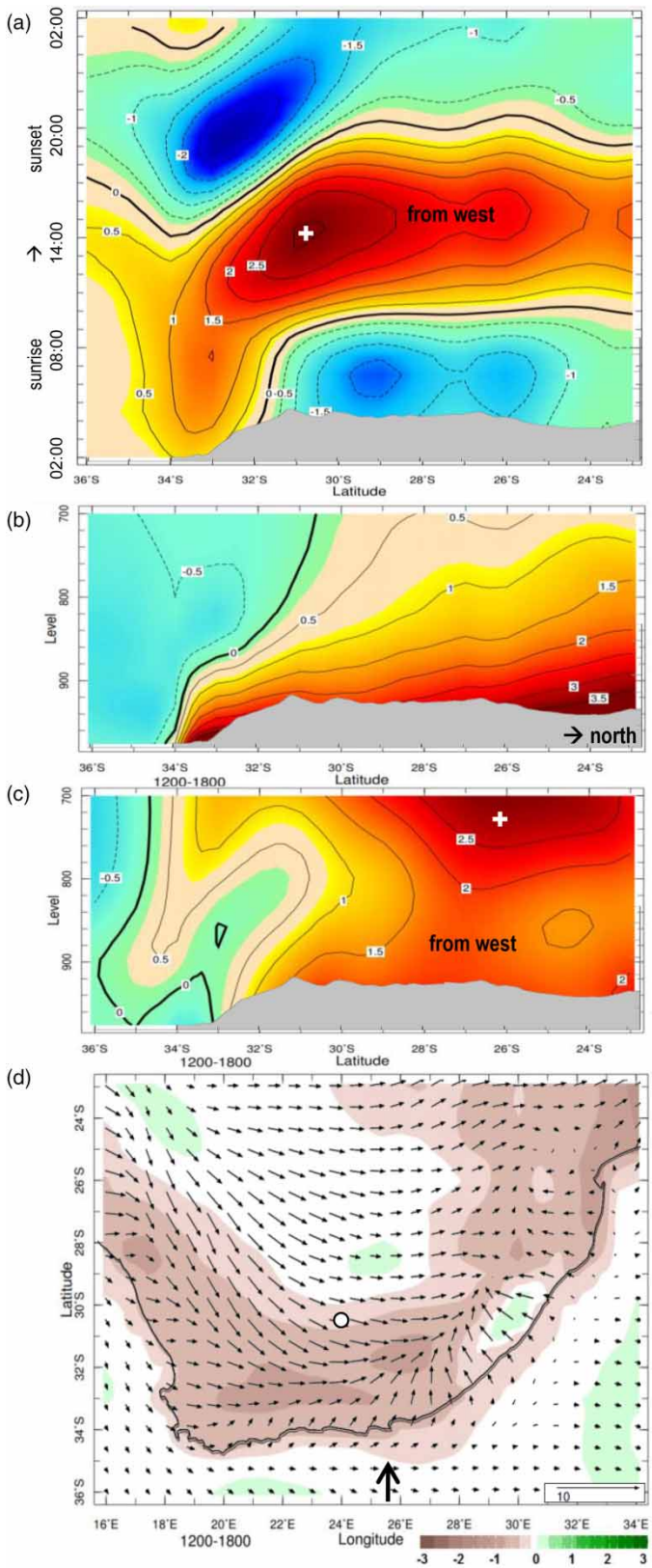

Figure 4 | (a) 2014–2019 mean diurnal cycle Hovmöller plot of low-level zonal winds (m/s) sliced along 25.5°E (time goes up). Height section on 25.5°E of 12–18 h mean diurnal residual of (b) air temperature (°C) and (c) zonal wind (m/s), with topographic profile. (d) Map of 12–18 h mean diurnal residual of low-level specific humidity (g/kg) and winds (m/s); dot shows DeAar weather station, and arrow is the axis of section.

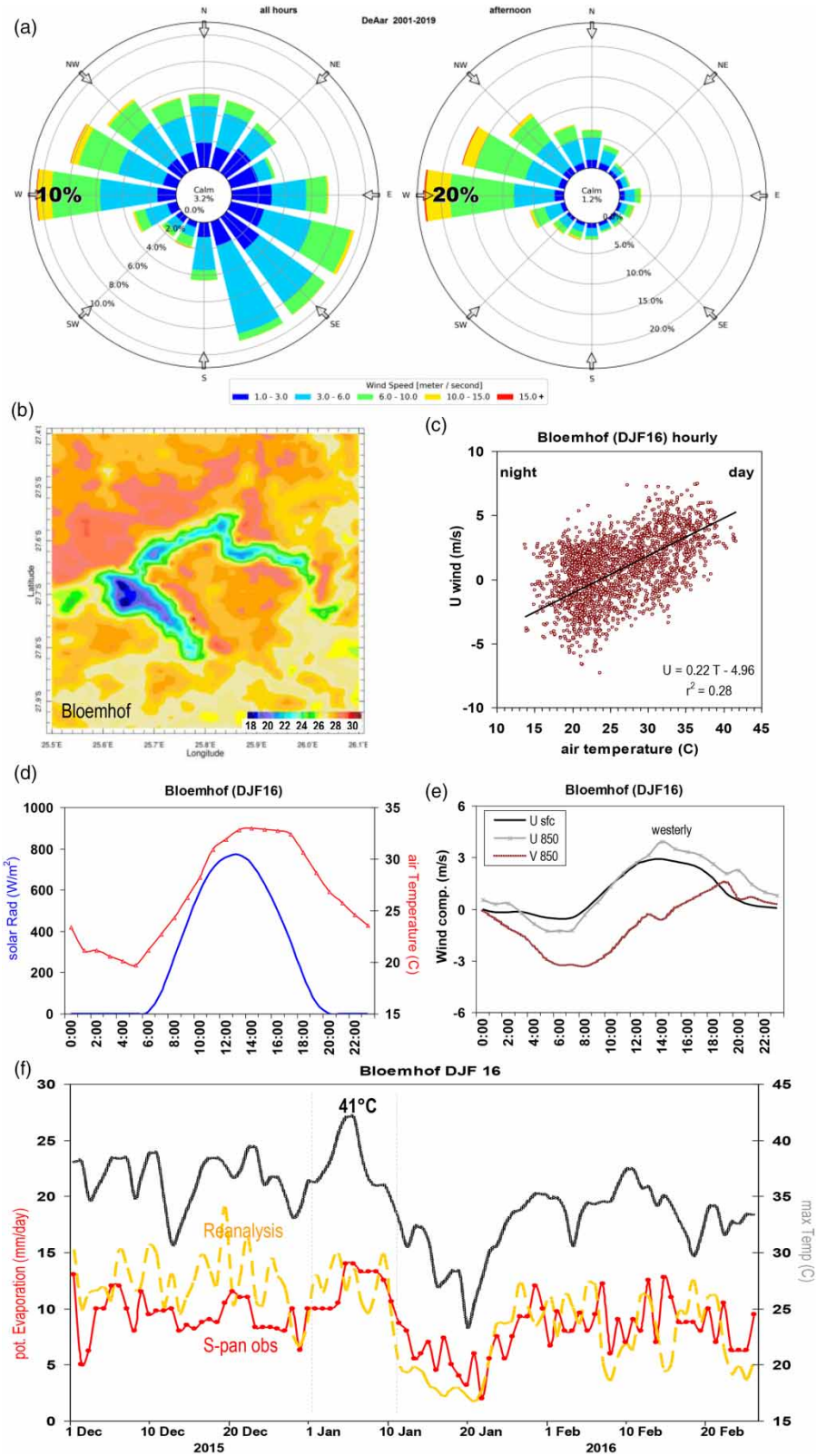

Figure 5 | (a) 2001–2019 DeAar wind rose (cf. Table 2 listing) comparing all hours (left) with 14:00–20:00 (right), %scale adjusted to maximum. (b) Bloemhof area mean surface temperature 2001–2019. DJF16 season: (c) scatterplot of hourly air temperature and zonal wind. DJF16 mean diurnal cycle: (d) net solar radiation and air temperature, (e) low-level winds, $N = 91$ per hour. (f) Daily record of station T_{max} (gray) and S-pan potential evaporation (red) just east of Bloemhof compared with reanalysis (gold). Dry case enclosed by dashed lines. Please refer to the online version of this paper to see this figure in color: http://dx.doi.org/10.2166/wcc.2021.187.

Table 2 | Wind probabilities at DeAar (Figure 5(e))

Calm 3.2% Mean 4.4 m/s						Calm 1.2% Mean 5.8 m/s					
Direction	**1.0–2.9**	**3.0–5.9**	**6.0–9.9**	**10.0–14.9**	**15.0+**	**Direction**	**1.0–2.9**	**3.0–5.9**	**6.0–9.9**	**10.0–14.9**	**15.0 +**
348-010°	1.86	2.77	0.91	0.03	0.00	348-010°	1.37	3.58	1.28	0.09	0.01
011-032°	1.61	2.66	0.96	0.04	0.00	011-032°	1.00	2.14	0.86	0.07	0.00
033-055°	2.27	1.90	0.46	0.04	0.00	033-055°	0.64	0.96	0.48	0.07	0.00
056-077°	2.10	1.06	0.24	0.02	0.00	056-077°	0.67	0.87	0.32	0.03	0.00
078-100°	2.99	2.60	1.55	0.11	0.00	078-100°	0.82	1.64	0.91	0.16	0.00
101-122°	2.53	3.67	3.02	0.25	0.01	101-122°	0.46	0.99	1.01	0.13	0.03
123-145°	3.03	5.02	1.06	0.04	0.00	123-145°	0.47	0.86	0.51	0.04	0.01
146-167°	1.86	6.84	0.54	0.02	0.00	146-167°	0.55	0.83	0.33	0.03	0.00
168-190°	1.11	2.50	0.76	0.02	0.00	168-190°	0.78	1.34	0.59	0.02	0.00
191-212°	0.42	0.76	0.74	0.15	0.01	191-212°	0.52	1.10	1.04	0.29	0.04
213-235°	0.52	0.82	0.45	0.06	0.00	213-235°	0.55	1.56	1.04	0.18	0.01
236-257°	0.74	1.72	0.78	0.13	0.01	236-257°	0.70	2.64	2.07	0.36	0.04
258-280°	1.40	4.29	3.63	1.07	0.06	258-280°	1.52	**6.64**	**10.38**	3.96	0.23
281-302°	1.07	3.44	3.06	0.61	0.04	281-302°	1.04	**5.58**	**8.30**	2.16	0.14
303-325°	1.31	3.38	2.02	0.19	0.01	303-325°	1.28	**5.37**	4.90	0.64	0.03
326-347°	1.27	2.75	1.39	0.08	0.00	326-347°	1.02	3.89	2.38	0.18	0.02

In 2001–2019, all hours (left, *N*~46,000) and afternoon 14:00–20:00 h (right, *N*~12,000); percentage per category: direction (rows) and speed (column, m/s). Bold values highlight afternoon westerlies >5%, which advect dry air across South Africa.

The diurnal cycle at the Bloemhof Reservoir (Figure 5(b)) is analyzed. The DJF16 summer scatterplot of hourly air temperature and zonal wind (Figure 5(c)) illustrates that day-time temperatures of >35 °C support westerly airflow (+U) and nighttime temperatures of <20 °C promote easterly airflow (–U) with some dispersion that achieves a linear regression $r^2 = 0.28$. Mean diurnal air temperatures crest at 33 °C from 13:00 to 18:00 h (Figure 5(c)). Westerlies accelerate +3 m/s during the afternoon, while northerlies –3 m/s prevail near sunrise and weaken at other times (Figure 5(d)).

Daily records of maximum temperature and potential evaporation (Figure 5(e)) reflect drought conditions in DJF16, relieved by only one cool wet spell. Potential evaporation follows Tmax, and reanalysis compares well with S-pan observations near Bloemhof. Moisture losses from 1 December 2015 to 10 January 2016 exceeded 10 mm/day.

3.3. Dry case

Hourly time series of reanalysis variables at Bloemhof during the dry spell of 1–10 January 2016 (Figure 6(a)) illustrate a 20 mm/day diurnal cycle for sensible heat flux, while latent heat fluxes remained ~2 mm/day: evaporation exceeded transpiration by an order of magnitude. Afternoon heating deepened the boundary layer to 4+ km, and zonal winds oscillated from –5 to +5 m/s in phase. Soil moisture depleted from 32 to 15% as specific humidity dipped below 4 g/kg during afternoon westerlies.

The 14:00 6 January 2016 map of wind and temperature (Figure 7(d)) illustrates a near-surface westerly flow of 10 m/s across the plateau, as a frontal system swept along the coast introducing air temperatures of <15 °C in contrast with the interior of >30 °C. The height section (Figure 7(e)) demonstrates 'uptake' of the sub-tropical jet over the Kalahari; axes of concentrated westerly flow prevail in the 800 hPa layer at 31 and 27°S, within a 4+ km deep atmospheric boundary layer. The Bloemfontein (FABL) radiosonde profile (Table 3) had convective inhibition of −68 J/kg and 9 m/s westerly winds near 800 hPa advecting air with a dewpoint depression of 22 °C.

3.4. Temporal trends

If the Bloemhof area has been over-run by a drier climate, then trends should be evident in long-term records of temperature and river discharge, as noted in Zou *et al.* (2019). A large seasonal cycle dominates the linear trend in satellite measured surface temperatures (Figure 7(a)). Day-time values oscillate between 20 and 40 °C with weak upward trends (+1 °C/18 years).

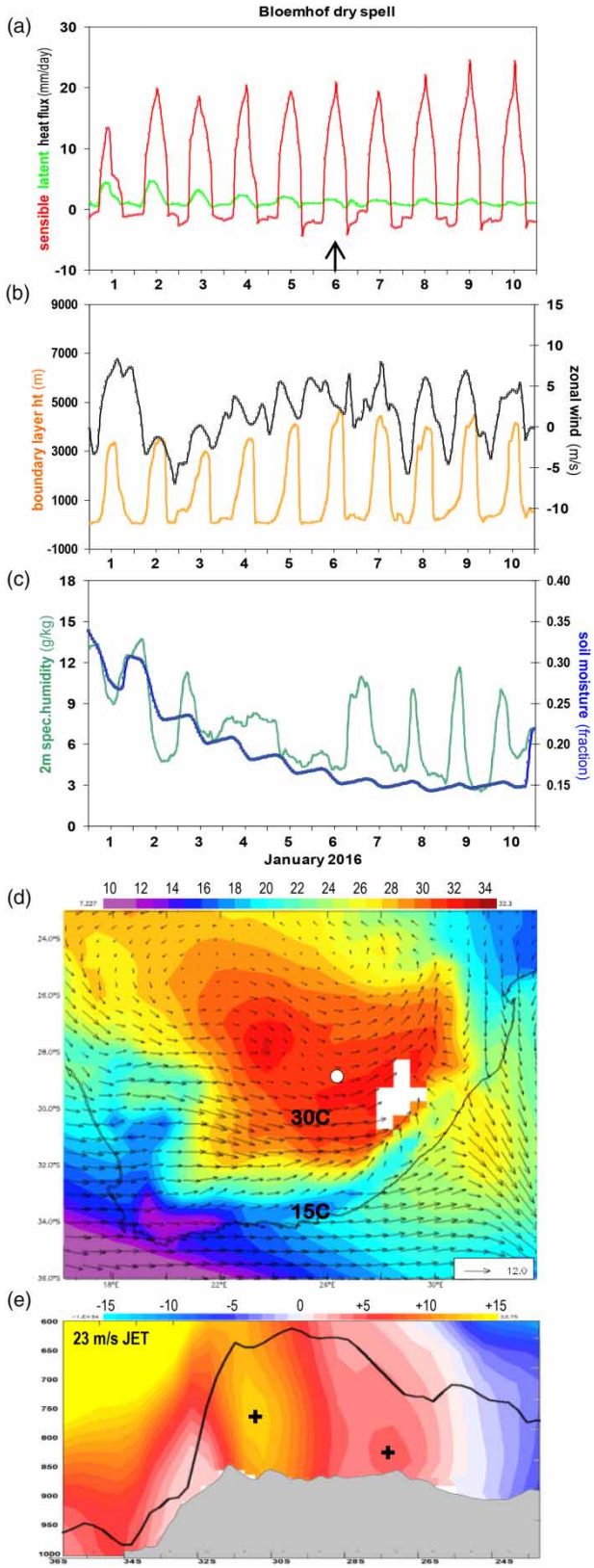

Figure 6 | (a–c) Temporal record of hourly near-surface reanalysis weather variables at Bloemhof during the dry spell. 14:00 6 January 2016: (d) map of 800 hPa air temperature and wind and (e) height section of zonal wind (shaded) and boundary layer height (line) on 25.5°E. Dot in (d) refers to Bloemfontein radiosonde (Table 3).

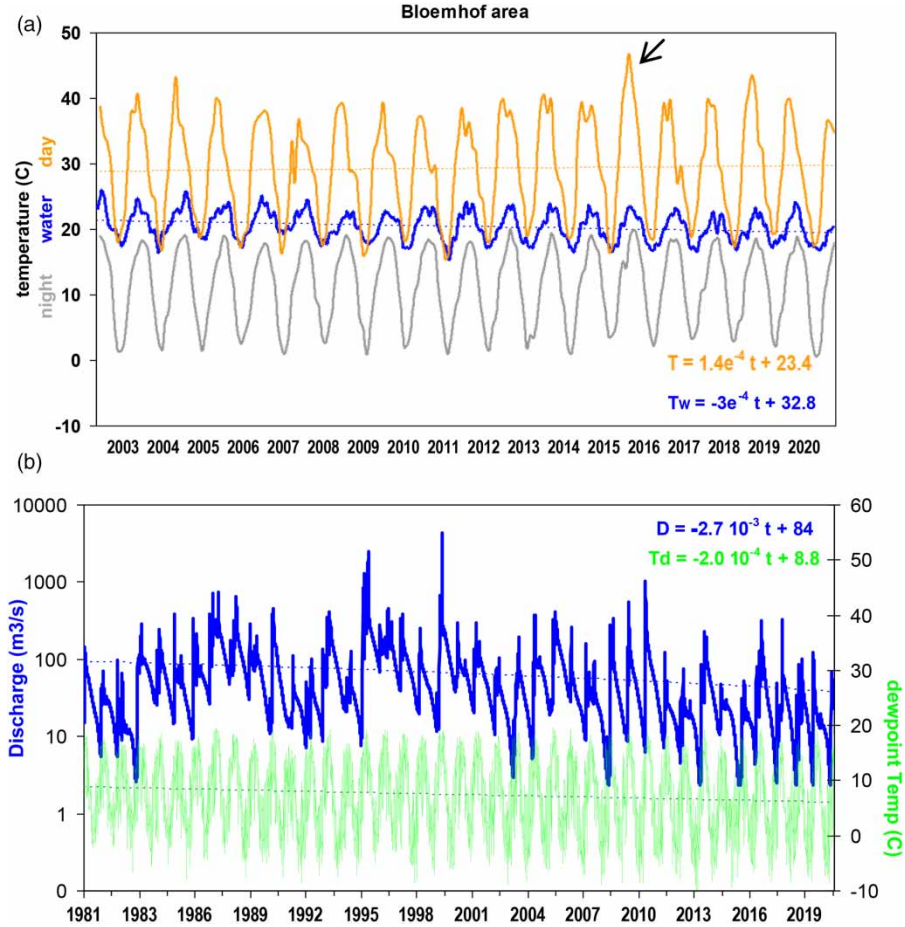

Figure 7 | Temporal record of Bloemhof area: (a) satellite night/water/day surface temperatures 2003+ (weekly de-clouded), and (b) daily river discharge and dewpoint temperature. Arrow points to dry case; linear trends are given, where t = days and seasonal cycle is retained so r^2 <0.05.

Night-time temperatures reach 0 °C every winter and have no significant trend. The Bloemhof Reservoir water temperatures actually declined –1 °C over the period 2003–2020, consistent with Tveg that showed little warming over the central plateau (cf. Figure 2(b)). Naturalized river discharge surges every summer and draws down in the winter, as T_d falls below 0 °C (Figure 7(b)). The beginning and endpoints of the regression line over 40 years have declined from 85 to 45 m^3/s (discharge) and from 8.2 to 6.4 °C for T_d. Discharge fell to 2.3 m^3/s on 6 January 2016, as Bloemfontein (FABL) measured an all-time record of 31.2% relative humidity in December 2015, suggesting that drying trends outpace warming trends.

3.5. Hydrology projections

The HADgem2-ISIMIP hydrology projections of potential evaporation 1981–2099 are evaluated. The filtered temporal record at Bloemhof (Figure 8(a)) shows that submodels exhibit a variety of responses. All trends are upward about 1 mm/day with the linear regression fit r^2 of 0.71 (LPjml) and 0.86 (Watergap). Large interannual fluctuations of potential evaporation in H08 overwhelm the trend r^2 of 0.12; dry spells exhibit periods of 3, 5, and (after 2060) 8 years. The LPjml pattern (Figure 8(b)) has an SW-NE alignment similar to cloud fraction (cf. Figure 3(b)) and shows poleward contraction of sub-humid conditions toward the Eastern Cape. The Watergap pattern of potential evaporation (Figure 8(c)) resembles ERA5 (cf. Figure 3(a)) and shows little movement of the semi-arid boundary. Instead, moisture deficits spread into the Limpopo, Lubombo, and Tugela Valleys. Watergap is drier than LPjml and ERA5 along the southern coast (Langeberg and Karoo), but over the plateau, it simulates gradual climate change.

Table 3 | Radiosonde profile at Bloemfontein 09Z 07 January 2016

Pressure hPa	Height m	Temperature °C	Dewpoint °C	Humidity g/kg	Direction °	Speed m/s	θe K
863	1,354	36.6	6.6	7.13	240	4	346.6
857	1,427	32.6	4.6	6.24	258	5	339.9
850	1,512	31.8	4.8	6.38	280	5	340.3
792	2,137	25.9	2.8	5.94	265	**9**	339.1
776	2,318	24.2	2.2	5.81	263	**9**	338.7
709	3,096	16.6	−0.4	5.27	256	8	337.0
700	3,205	15.6	−0.4	5.34	255	8	337.3
653	3,787	10.0	−2.0	5.09	270	10	336.6
610	4,347	5.8	−3.2	4.98	283	14	337.8
602	4,454	4.9	−3.5	4.94	285	15	337.8
571	4,883	1.4	−4.6	4.79	292	16	338.2
559	5,052	−0.3	−5.5	4.57	295	16	337.4
542	5,298	−2.7	−6.8	4.26	294	17	336.4
513	5,730	−6.5	−9.0	3.79	291	17	335.5
501	5,915	−7.9	−11.9	3.08	290	18	333.7
500	5,930	−8.1	−12.0	3.06	290	18	333.6

CAPE (convective available potential energy), 41.61 J/kg, CIN (convective inhibition), −68.41 J/kg, Prec Wtr (precipitable water), 21.94 mm. Kalahari westerlies highlighted in bold.

3.6. Quantitative analysis

The above description is quantified by the analysis of sub-humid zone contraction over time. From Figure 3, the before and after 2001 changes (# 0.5° squares) are cloud fraction of 160–112, potential evaporation of 114–83, and vegetation temperature of 97–42. From Figure 8, the changes in area (#) in 20th and 21st century projected potential evaporation are LPjml of 124–50 and Watergap 105–38, a significant contraction of the sub-humid zone between the escarpment and southeast coast (Agulhas Current).

Considering the eastward expansion of the semi-arid edge from longitude of 25.5°E, the before and after 2001 changes (# 0.5° squares) are cloud fraction of 34–90, potential evaporation of 58–78, and vegetation temperature of 72–118. The eastward expansion of the semi-arid edge in the 20th and 21st century projected potential evaporation (#) are LPjml of 64–128 and Watergap 61–80. Despite the subjective nature of threshold analysis (Quetin & Swann 2017), the evidence points to a southeastward shift of moisture deficits over the South African plateau, consistent with Engelbrecht & Engelbrecht (2016). Figure 9(a) elucidates the process linking cause and effect.

3.7. Projected thermal winds

Using HADgem2 projections along 25.5°E for potential temperature and zonal wind in the 20th and 21st centuries, warming off the south coast is only 1.3 °C associated with a ~1 m/s weakening of westerly winds (and upwelling, Figure 2(g)). Over the escarpment, the RCP6 scenario yields a potential temperature increase of 4.9 °C associated with a 0.5 m/s strengthening of westerly winds. Further north, the warming moderates, and surface easterlies prevail.

Coupled model projections indicate that the escarpment may warm at double the rate of the coast. The intensified meridional temperature gradient could enhance the sub-tropical jet (Figure 9(b)) and deliver anticyclonic vorticity such as may occur during the Pacific El Niño phase. Despite projections of enhanced easterly flow along the coast (Figure 9(c)), westerlies over the plateau could spread dry air from the Kalahari Desert (Vigaud *et al.* 2009) into the Vaal River catchment. The warming of vegetation around the perimeter of South Africa (+0.2 °C/year, cf. Figure 2(b)) may inhibit local moisture recycling and compound the more westerly circulation.

4. CONCLUSIONS

African climate change is well studied particularly for seasonal rainfall and temperature from station interpolations. Using low precipitation thresholds (0.3 mm/day), the Kalahari Desert showed little change over the 20th century (Thomas &

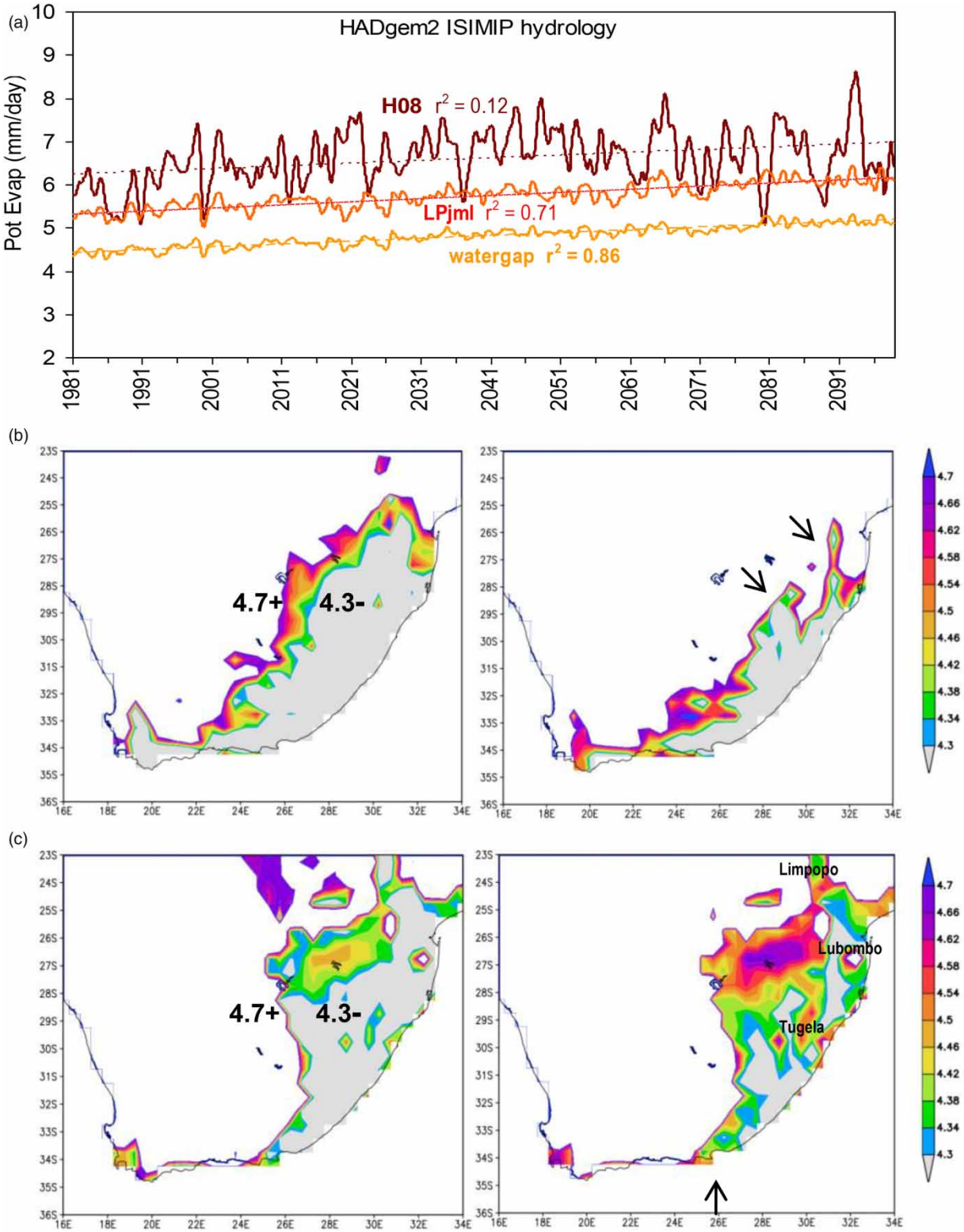

Figure 8 | HADgem2-ISIMIP projections with RCP6 scenario at the Bloemhof reservoir: (a) filtered temporal record and trend from three submodels. Maps of projected potential evaporation for semi-arid thresholds, 1981–2000 (left) and 2080–2099 (right): (b) LPjml (with eastern valleys labeled) and (c) watergap, compared with Figure 3. Arrow in (c) refers to the axis of (Figure 9(a)).

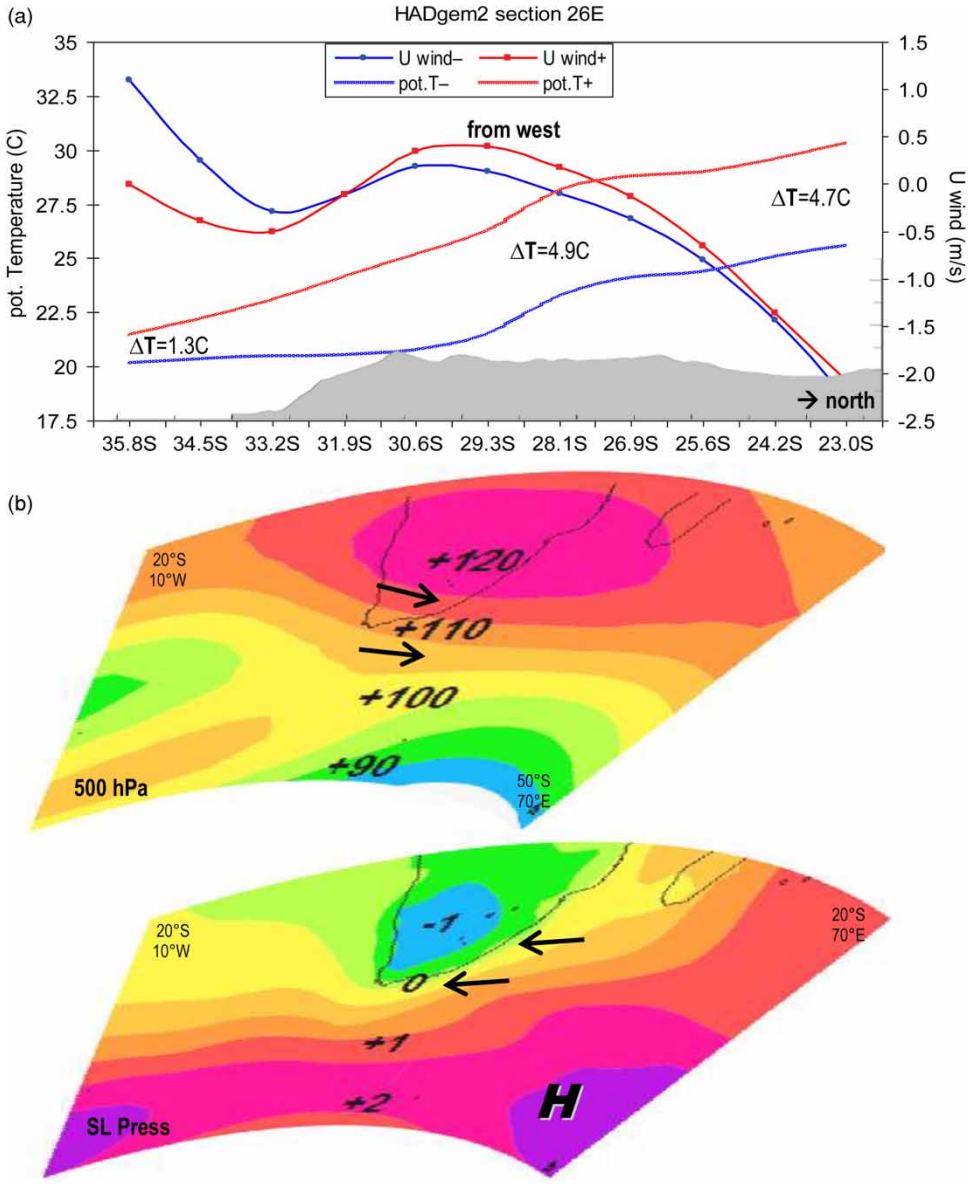

Figure 9 | (a) HADLEYgem2 projections for 1981–2000 blue– and 2080–2099 red+ on north-south axis 25.5°E of near-surface potential temperature and zonal wind, with topographic profile and 100 year delta temperature. (b) HADLEYgem2 projected difference 2080–2099 minus 1981–2000 for 500 hPa geopotential height (m) and sea-level pressure (lower, hPa). Arrows indicate circulation changes. Please refer to the online version of this paper to see this figure in color: http://dx.doi.org/10.2166/wcc.2021.187.

Nigam 2018). Similarly, Mayaud *et al.* (2017) found that changes in vegetation cover in 21st century projections depend on land use. Here, it was recognized that semi-arid zones are dominated by year-round evaporative stress. Thus, a different approach was taken, using satellite assimilated semi-arid thresholds for annual evaporation, and investigating links between boundary layer coupling and the atmospheric circulation from diurnal to centennial timescales.

A trend toward westerly airflow (Figure 2(g)) is drying the South African Highveld, so cloud fraction has declined, and potential evaporation and vegetation temperature have risen. Changes in coastal climate were related to east-west differences in trends of shelf SST: a warmer Agulhas Current and cloudy weather contrasted with Benguela upwelling under sunny skies. Although trends may be aliased by multi-decadal oscillations (Johnson *et al.* 2020), the South African climate response to rising greenhouse gases led to similar outcomes from 40 year observation records and 100+ year coupled model projections (Figures 3(c) and 9(a)) consistent with Engelbrecht & Engelbrecht (2016). Satellite estimated evaporation and cloud cover

demonstrated a shift in the semi-arid boundary from 25 to 27°E underpinned by a diurnal outpouring of dry air from the Kalahari Desert (Figure 4(d)). The HADgem2-ISIMIP hydrology projections continued the drying trend and, together with a case study, gave insights on how the sub-tropical jet is attracted to South Africa (Figures 7(b) and 9(b)).

The statistical analysis of potential evaporation fields revealed that semi-arid conditions expanded eastward from 25.5°E from #58 (2001−) to #78 (2001+), consistent with coupled model projections from #61 to #80 by 2100, yielding a 50,000 km^2 expansion of semi-arid conditions. Highveld croplands may transition to grazing, as agricultural and water resources shift southeastward. The sub-humid zone is contracting, especially in east-facing valleys (Figures 3(c) and 8(c)). These outcomes suggest that boosting Eastern Cape agricultural productivity could alleviate scarcity. Although rainfall may hold steady, mitigating actions should plan for evaporative stress (Challinor *et al.* 2014).

ACKNOWLEDGEMENTS

SAPSE support from the South Africa Dept of Education is acknowledged. Data were analyzed from the IRI Climate Library, KNMI Climate Explorer, Univ. Hawaii APDRC, Univ. Wyoming Radiosonde, Iowa State Environmental Monitoring, and Dept Water Affairs (SA). An excel spreadsheet of data analysis is available on request.

DATA AVAILABILITY STATEMENT

All relevant data are included in the paper or its Supplementary Information.

REFERENCES

Bounoua, L., Collatz, G. J., Los, S. O., Sellers, P. J., Dazlich, D. A., Tucker, C. J. & Randall, D. A. 2000 Sensitivity of Climate to Changes in NDVI. *Journal of Climate* **13**(13), 2277–2292.

Challinor, A., Watson, J., Lobell, D., Howden, S. M., Smith, D. R. & Chhetri, N. 2014 A meta-analysis of crop yield under climate change and adaptation. *Nature Climate Change* **4**, 287–291.

Chikoore, H. & Jury, M. R. 2010 Intra-seasonal variability of satellite derived rainfall and vegetation over Southern Africa. *Earth Interactions* **14**, 1–26.

Engelbrecht, C. J. & Engelbrecht, F. A. 2016 Shifts in Köppen-Geiger climate zones over Southern Africa in relation to key global temperature goals. *Theoretical Applied Climatology* **123**, 247–261.

Eumetsat 2021a CM-SAF algorithm theoretical basis document: CLARA-A2 surface radiation. Trentman, J. (lead author), SAF/CM/DWD/ICDR/CLARA/RAD/ATBD.

Eumetsat 2021b CM-SAF algorithm theoretical basis document: CLARA-A2 fractional cloud cover. Karlsson, K.-G. (lead author), SAF/CM/DWD/ICDR/CLARA/CLD/ATBD.

Frieler, K., Lange, S., Piontek, F., Reyer, C. P. O., Schewe, J., Warszawski, L., Zhao, F., Chini, L., Denvil, S., Emanuel, K., Geiger, T., Halladay, K., Hurtt, G., Mengel, M., Murakami, D., Ostberg, S., Popp, A., Riva, R., Stevanovic, M., Suzuki, T., Volkholz, J., Burke, E., Ciais, P., Ebi, K., Eddy, T. D., Elliott, J., Galbraith, E., Gosling, S. N., Hattermann, F., Hickler, T., Hinkel, J., Hof, C., Huber, V., Jägermeyr, J., Krysanova, V., Marcé, R., Müller Schmied, H., Mouratiadou, I., Pierson, D., Tittensor, D. P., Vautard, R., van Vliet, M., Biber, M. F., Betts, R. A., Bodirsky, B. L., Deryng, D., Frolking, S., Jones, C. D., Lotze, H. K., Lotze-Campen, H., Sahajpal, R., Thonicke, K., Tian, H. & Yamagata, Y. 2017 Assessing the impacts of 1.5 °C global warming - simulation protocol of the Inter-Sectoral Impact Model Intercomparison Project (ISIMIP2b). *Geosci. Model Dev.* **10**, 4321–4345.

Hanasaki, N., Kanae, S., Oki, T., Masuda, K., Motoya, K., Shirakawa, N., Shen, Y. & Tanaka, K. 2008 An integrated model for the assessment of global water resources - Part 2: Applications and assessments. *Hydrol. Earth Syst. Sci.* **12**, 1027–1037.

Harrigan, S., Zsoter, E., Alfieri, L., Prudhomme, C., Salamon, P., Wetterhall, F., Barnard, C., Cloke, H. & Pappenberger, F. 2020 GloFAS-ERA5 operational global river discharge reanalysis 1979-present. *Earth Syst. Sci. Data* **12**, 2043–2060.

Hersbach, H., Bell, B., Berrisford, P., Hirahara, S., Horányi, A., Muñoz-Sabater, J., Nicolas, J. P., Peubey, C., Radu, R., Schepers, D., Simmons, A. J., Soci, C., Abdalla, S., Abellan, X., Balsamo, G., Bechtold, P., Biavati, G., Bidlot, J., Bonavita, M., Chiara, G. D., Dahlgren, P., Dee, D., Diamantakis, M., Dragani, R., Flemming, J., Forbes, R. G., Fuentes, M., Geer, A. J., Haimberger, L., Healy, S. B., Hogan, R. J., Holm, E. V., Janisková, M., Keeley, S. P., Laloyaux, P., Lopez, P., Lupu, C., Radnoti, G., Rosnay, P. D., Rozum, I., Vamborg, F. S., Villaume, S. & Thepaut, J. 2020 The ERA5 global reanalysis. *Quarterly Journal of the Royal Meteorological Society* **146**, 1999–2049.

Jägermeyr, J., Gerten, D., Heinke, J., Schaphoff, S., Kummu, M. & Lucht, W. 2015 Water savings potentials of irrigation systems: global simulation of processes and linkages. *Hydrol. Earth Syst. Sci.* **19**, 3073–3091.

Johnson, N. C., Amaya, D. J., Ding, Q., Kosaka, Y., Tokinaga, H. & Xie, S.-P. 2020 Multidecadal modulations of key metrics of global climate change. *Global Planetary Change* **188**, 103149. doi:10.1016/j.gloplacha.2020.103149.

Jury, M. R. 2016 Climate influences on Vaal River flow. *Water SA* **42**, 232–242.

Jury, M. R. 2018 Climate trends across South Africa since 1980. *Water SA* **44**, 297–307.

Keys, P. W., Wang-Erlandsson, L. & Gordon, L. J. 2016 Revealing invisible water: moisture recycling as an ecosystem service. *PLoS ONE* **11**, e0151993. doi:10.1371/journal.pone.0151993.

Mann, M. E., Steinman, B. A. & Miller, S. K. 2020 Absence of internal multidecadal and interdecadal oscillations in climate model simulations. *Nature Communications* **11**, 49. doi:10.1038/s41467-019-13823-w.

Mayaud, J. R., Bailey, R. M. & Wiggs, G. F. 2017 Modelled responses of the Kalahari Desert to 21st century climate and land use change. *Science Reports* **7**, 3887. doi:10.1038/s41598-017-04341-0.

Molod, A., Takacs, L., Suarez, M. & Bacmeister, J. 2015 Development of the GEOS-5 atmospheric general circulation model: evolution from MERRA to MERRA2. *Geoscience Model Development* **8**, 1339–1356.

Müller, S. H., Eisner, S., Franz, D., Wattenbach, M., Portmann, F. T., Flörke, M. & Döll, P. 2014 Sensitivity of simulated global-scale freshwater fluxes and storages to input data, hydrological model structure, human water use and calibration. *Hydrol. Earth Syst. Sci.* **18**, 3511–3538.

Munday, C. & Washington, R. 2018 Systematic climate model rainfall biases over Southern Africa: links to moisture circulation and topography. *Journal of Climate* **31**, 7533–7548.

NESDIS 2021 *Vegetation Condition Products Based on NOAA Satellite Radiance*. Available from: www.star.nesdis.noaa.gov/smcd/emb/vci/VH/VH-Syst_10ap30.php, www.star.nesdis.noaa.gov/smcd/emb/vci/VH/vh_browse.php.

Quetin, G. R. & Swann, A. L. S. 2017 Empirically derived sensitivity of vegetation to climate across global gradients of temperature and precipitation. *Journal of Climate* **30**, 5835–5849.

Rienecker, M. M., Suarez, M. J., Gelaro, R., Todling, R., Bacmeister, J., Liu, E., Bosilovich, M. G., Schubert, S. D., Takacs, L., Kim, G., Bloom, S., Chen, J., Collins, D., Conaty, A., da Silva, A., Gu, W., Joiner, J., Koster, R. D., Lucchesi, R., Molod, A., Owens, T., Pawson, S., Pegion, P., Redder, C. R., Reichle, R., Robertson, F. R., Ruddick, A. G., Sienkiewicz, M. & Woollen, J. 2011. MERRA: NASA's Modern-Era Retrospective Analysis for Research and Applications. *Journal of Climate* **24**(14), 3624–3648.

Ringrose, S., Matheson, W., Wolski, P. & Huntsman-Mapila, P. 2003 Vegetation cover trends along the Botswana Kalahari transect. *Journal of Arid Environments* **54**, 297–317.

Saha, S., Moorthi, S., Pan, H., Wu, X., Wang, J., Nadiga, S., Tripp, P., Kistler, R., Woollen, J., Behringer, D., Liu, H., Stokes, D., Grumbine, R., Gayno, G., Wang, J., Hou, Y., Chuang, H., Juang, H. H., Sela, J., Iredell, M., Treadon, R., Kleist, D., Van Delst, P., Keyser, D., Derber, J., Ek, M., Meng, J., Wei, H., Yang, R., Lord, S., van den Dool, H., Kumar, A., Wang, W., Long, C., Chelliah, M., Xue, Y., Huang, B., Schemm, J., Ebisuzaki, W., Lin, R., Xie, P., Chen, M., Zhou, S., Higgins, W., Zou, C., Liu, Q., Chen, Y., Han, Y., Cucurull, L., Reynolds, R. W., Rutledge, G. & Goldberg, M. 2010 The NCEP Climate Forecast System Reanalysis. *Bulletin of the American Meteorological Society* **91**(8), 1015–1058.

Saha, S., Moorthi, S., Wu, X., Wang, J., Nadiga, S., Tripp, P., Behringer, D., Hou, Y., Chuang, H., Iredell, M., Ek, M., Meng, J., Yang, R., Mendez, M. P., van den Dool, H., Zhang, Q., Wang, W., Chen, M. & Becker, E. 2014 The NCEP Climate Forecast System Version 2. *Journal of Climate* **27**(6), 2185–2208.

Scholes, R., Dowty, P., Caylor, K., Parsons, D., Frost, P. & Shugart, H. 2002 Trends in savanna structure and composition along an aridity gradient in the Kalahari. *Journal of Vegetation Science* **13**, 419–428.

Taylor, K. E., Stouffer, R. J. & Meehl, G. A. 2011 An overview of CMIP5 and the experiment design. *Bulletin American Meteorological Society* **93**, 485–498.

Thomas, N. & Nigam, S. 2018 Twentieth-century climate change over Africa: seasonal hydroclimate trends and Sahara Desert expansion. *Journal of Climate* **31**, 3349–3370.

Tyson, P. D. & Crimp, S. J. 1998 The climate of the Kalahari transect. *Transactions Royal Society South Africa* **53**, 93–112.

Vigaud, N., Richard, Y., Rouault, M. & Fauchereau, N. 2009 Moisture transport between the South Atlantic Ocean and Southern Africa: relationships with summer rainfall and associated dynamics. *Climate Dynamics* **32**, 113–123.

Zou, S., Jilili, A., Duan, W., Maeyer, P. D. & deVoorde, T. V. 2019 Human and natural impacts on the water resources in the Syr Darya River Basin, Central Asia. *Sustainability* **11**, 3084. doi:10.3390/su11113084.

First received 9 May 2021; accepted in revised form 10 September 2021. Available online 1 October 2021